

X-Ray Shielding Characteristics of Sand Reinforced Plastic Concrete Blocks

^{1,*} Masok Felix Bitrus, ^{2,*} Umar Sa'ad Aliyu, ³Dawam Robert Rangmou, ⁴Amina Muhammad Dunama, ²Oni Samuel Tolulope

¹Department of Physics, Faculty of Natural and Applied Sciences, Plateau State University Bokkos, PMB 2012, Jos, Plateau State, Nigeria

²Department of Physics, Faculty of Sciences, Federal University of Lafia, P. M. B 146, Lafia, Nasarawa State, Nigeria

³Department of Physics, Faculty of Natural Science, University of Jos, PMB 2084, Jos, Plateau State, Nigeria

⁴Muhammadu Buhari TETFund Centre for Excellence, Federal University of Lafia, P. M. B 146, Lafia, Nasarawa State, Nigeria

*Corresponding Author: masokfelix@plasu.edu.ng, umar.aliyu@science.fulafia.edu.ng

Received: 1 November 2024; **Accepted:** 25 January 2025; **Published:** 4 February 2025

To cite this article (APA): Masok F.B, Umar S.A., & Dawam, R.R., Amina M.D., Oni S., T. (2025). X-Ray Shielding Characteristics of Sand Reinforced Plastic Concrete Blocks. EDUCATUM Journal of Science, Mathematics and Technology, 12(1), 148–162.

To link to this article:

Abstract

X-Ray shielding efficiency of sand reinforced plastic concrete blocks synthesized using sand and waste sachet water plastic in the percentage ratio of 50:50, 30:70, 10:90 and 0:100 has been studied in this paper. The density of the synthesized concrete blocks and their x-ray shielding characteristics were measured using a densitometer and a set of x-rays shielding fixed diagnostic x-ray machine and digital Geiger counter respectively. The density value decreased as the sand percentage decreased from 1.922 gcm^{-3} to 1.250 gcm^{-3} with an increasing plastic percentage, resulting from the substitution of sand with lighter plastic. The linear attenuation coefficient (LAC) and the mass attenuation coefficient (MAC) values increased with an increase in the percentage of plastic while the tenth value layer (TVL) and half value layer (HVL) decreased with increase in the percentage of plastic in the concrete material. The value of the mean free path (MFP) appeared higher when more sand composition. The results demonstrated that more plastic composition improved the concrete shielding efficiency even as the density continued to decrease. This might be since more spaces are closed with more plastic percentage, closing gaps between sand particles. The study demonstrated that the sand reinforced plastic concrete presented in this work offers greater advantage solves the problems of light weight and durability that is faced with conventional cement concrete materials in X-rays shielding applications.

Keywords: X-rays, Plastic waste, Concretes, Radiation shielding efficiency.

INTRODUCTION

Human exposure to both non-ionizing and ionizing radiation (includes X-rays, gamma rays and high energy particles) from both natural and artificial sources is inevitable, especially the natural ones that comprise of the cosmic showers and earth crust emissions [1]. The artificial activities such as nuclear medicine procedures (diagnostic and therapeutic), mining, space missions, nuclear power plants and others also contribute greatly to the level of exposure of humans to ionizing radiation [2][3].

Gamma and X-rays constitute a part of ionizing radiation with high energies and penetration powers [4]. This radiation possesses great potential to harm human health and damage sensitive equipment or materials around their vicinity. Thus, efficient shielding materials are required for the attenuation of these high energy radiations to levels of safety and acceptability. Traditionally, concrete blocks, tiles and clay bricks are used in shielding ionizing radiations [4][5].

In general, shielding characteristics and efficiency of any materials is dependent on the material's atomic number, density, radiation resistance shielding permanence, multi-use possibility, heat dissipation ability, obtainability and radiation level lowering ability [6]. Concretes materials, especially the cement concretes offer good shielding efficiency and cost effectiveness in X-ray room and general shielding applications, but is faced with some setbacks that include their durability (due to their permeability), microcracks occurrence resulting from related stresses and hydration heat, corrosion, carbonation and chloride ingress [7]. Lead, which proved to be efficient in shielding ionizing radiation have been used over the years for the ionizing radiation shielding application in various hospitals and nuclear centers around the world. The use of lead in such applications have faced serious opposition from experts, pointing the dangers of chemical toxicity [8]–[10].

Over the years, researchers have been trying explore alternative materials for radiation shielding applications, which include composites [11]–[15]. Polymer composite materials offer advantages such as lower weight, improved durability, and reduced environmental impact. Several studies have investigated the radiation shielding properties of polymer-based composites, including those reinforced with metal oxides, ceramics, and natural fibers [11], [16]. Sand-reinforced plastic concrete blocks have been identified as potential radiation shielding material due to their high density, low cost, and sustainability. However, limited research has been conducted on the radiation shielding properties of these blocks. In this paper, sand reinforced plastic concrete was synthesized and the X-ray shielding characteristic of the materials was studied and discussed.

MATERIALS AND METHODS

Preparation of Samples

Sand reinforced plastic/polymer concrete with varying sand content of 0 %, 10 %, 30 % and 50 % of total aggregate content. The bricks were made by using granulated plastics waste and sand. Mixtures matching the intended compositions were weighed using an Adam PW 184 (180X0.0001g) AE437713 electronic digital scale with an error measurement of ± 0.0001 g in accordance with equation. The components were vigorously mixed after heating and melting the

plastics in a breaker on an electronic stove before adding the sand sample. Proper mixing was done until homogenous mixture was obtained before pouring the mixture into the mold with thickness of 1 inch.

Table 1: Sample Composition and Labels

Samples	Sand(g)	Plastic(g)
S1	50	50
S2	30	70
S3	10	90
S4	0	100



Figure 1: Sample sand and Plastics Used

Density Measurement Procedure

Densities of all bricks were measured by using the Archimedes' principle which involves the weighting of glass in air and in distilled water at room temperature. The difference between these two masses were measured using digital electronic densimeter MH-300A with accuracy ± 0.0001 g. Serial number 20230409001-2, Model number MH-300A, manufacturing date 2023/04/10.



Figure 2: Density Measurement Procedure

The density ρ of the synthesized plastic-based concretes were measured using a densitometer model. The density resolution will be estimated at around $\pm 0.001 \text{ gcm}^3$. For each of the samples, the density will be determined using the Archimedes method where distilled water is the immersion liquid using the following relationship at room temperature using

$$\rho_{\text{sample}} = \frac{W_1}{W_2} \rho_{\text{water}} (\text{gcm}^{-3}) \quad (1)$$

Where ρ = is the density, W_1 is the weight of sample in air and W_2 is the weight of sample in water [17].

X-ray Attenuation Experiment

The setup for the radiation shielding experiment was done in line with the method reported by Kaewjaeng et al. [22] as shown in Figure 3. The holder was positioned at 40 cm from the X-ray tube while the detector probe was placed 100 cm away from the tube. The generated X-ray beams were collimated to 1.5 cm by 1.5 cm in the machine accompanying collimator.

Radiation Shielding Calculations

The total cross-section of radiation contact with an atom is equal to the sum of the cross-sections of the particle, photoelectric effect (τ), Compton Scattering (σ) and pair production (κ), depending on the photon energy and the absorbing material. By either absorbing them or scattering them, each impact eliminates photons. In the absorber, this relationship is defined as the likelihood of occurrence per unit path length. The Linear Attenuation Coefficient (LAC) can be desired as the interaction's full potential [18]; [19].

$$\mu = (\tau) + (\sigma) + (\kappa) \quad (2)$$

Linear Attenuation Coefficient (LAC)

When radiation is flowing through a material, the linear attenuation coefficient (μ) reduces the radiation's intensity. When radiation passes through a substance, the substance's electrons absorb some of the energy. Therefore, LAC is dependent on the physical state of the material. Therefore, using narrow beam geometry, Beer-Lambert's law can be used to calculate the attenuation of X-rays or gamma rays [20].

$$I = I_0 e^{-\mu t} \quad (3)$$

Where I_0 = the initial photon intensity, I = the transmitted photon intensity, t is the penetration depth (cm), and μ is the linear attenuation coefficient.

Mass Attenuation Coefficient (MAC)

Since LAC depends on the density of a material. Therefore, MAC is being used for practical purposes. The Mass Attenuation Coefficient values of the glasses will be evaluated by applying mixture rule of photons can be estimated from measured values of μ and ρ as follows:

$$\mu_m = \mu / \rho \quad (4)$$

Where ρ is the density of the material and μ is the linear attenuation coefficient [2].

The Mass Attenuation Coefficient of the glasses will be evaluated by the transmission method according to Lambert-Beer's law, equation (4). Which accounts for the radiation flux distribution when the ideal Lambert-Beer law conditions did not fulfil in the experimental conditions or setup [20], [21].

Half Value Layer (HVL) and Tenth Value Layer (TVL)

Half value layer and Tenth Value Layer is the thickness at which the transmitted intensity is reduced to 50% and 90% the initial intensity [20]. Lower HVL/TVL and MFP values allow for the production of better shielding materials. In the HVL & TVL are the thicknesses of radiation shielding material required. The material's capacity to block radiation increases with decreasing HVL and TVL values. The HVL of any material is the metric that determines the effectiveness of X-ray or gamma-ray shielding and expressed as:

$$HVL = \frac{\ln(2)}{\mu} \quad (5)$$

Where HVL is the half value layer

$$TVL = \frac{\ln(10)}{\mu} \quad (6)$$

Mean Free Path (MFP)

The MFP, which is the mean distance required to attenuate photons is an absorber calculated from the LAC as follows:

$$MFP = \frac{1}{\mu} \quad (7)$$

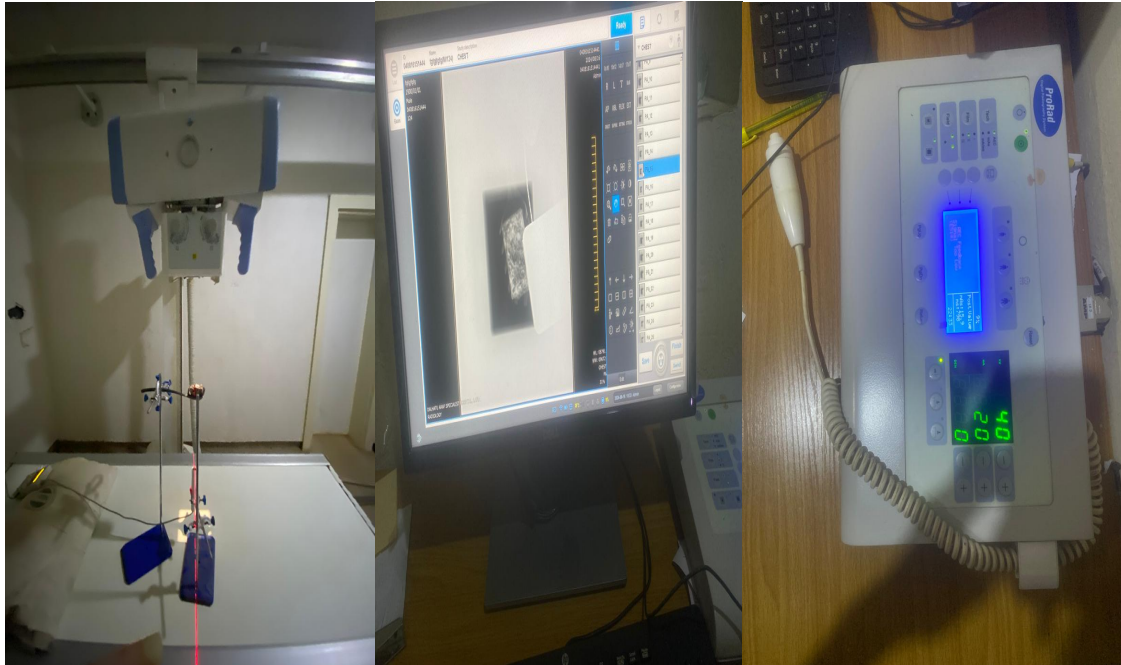


Figure 3: Experimental X-ray-up for Radiation Shielding Measurement

RESULTS AND DISCUSSIONS

Fabrication of radiation attenuating bricks system using sand and plastics waste was successful, as shown in Figure 4 below. The following characterization such density and radiation attenuation properties were carried to test the radiation ability of the bricks.



Figure 4: Fabricated Sand Reinforced Plastic Concrete Samples

Density of Synthesized Sand Reinforced Plastic Concrete

Using Archimedes method, the weight of an object in air W_1 / weight an object in water W_2 using DI water is used as immersed fluid at room temperature. The results show a decrease in density from 1.922 to 1.250 (gcm^{-3}) for bricks. The results displayed decrease is due to reduction of the sand sample and increase of the plastics content. As shown in Table 2 and Figure 5.

Table 2: Density Measurement Data

Samples	1	2	3	Total Average
S1	1.914	1.918	1.934	1.922
S2	1.434	1.446	1.464	1.448
S3	1.347	1.361	1.349	1.352
S4	1.221	1.262	1.268	1.250

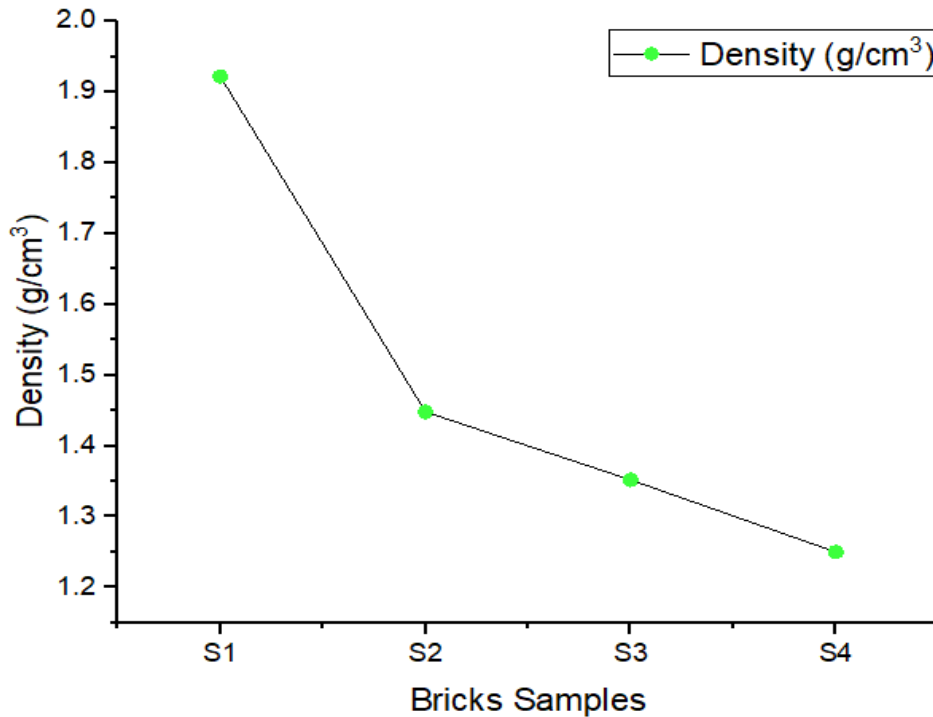


Figure 5: Density Plot for the Synthesized Plastic Concrete Samples

X-ray Attenuation Properties of Sand Reinforced Plastic Concrete

Attenuation efficiency of the new block series was investigated against low energy photons using diagnostic X-ray machine the evaluation of some parameters like LAC, MAC, HVL & TVL, and MFP. The blocks samples are S1 (50:50), S2 (30:70) S3 (10:90) and S4 (0:100) of sand to plastic ratio.

Table 3: Radiation Dose for the Synthesized Plastic Concrete Samples

Energy (kVp)	Background	S1	S2	S3	S4
80.00	1.68	0.92	0.70	0.5673	0.61
70.00	1.46	0.81	0.53	0.468	0.43
60.00	1.27	0.72	0.47	0.355	0.426
50.00	1.19	0.43	0.44	0.3904	0.384
40.00	0.57	0.46	0.31	0.396	0.336

Linear (LAC) and Mass Attenuation (MAC) Coefficients

LAC is a useful parameter used to determine the X-ray radiation attenuation shielding of any sample. As we can recall from equation (3) linear attenuation coefficient is the combination of interaction cross sections for photoelectric effect, Compton scattering and pair production, which are the three most important principles of photon attenuation in materials. Figures 6 and 7 present LAC and MAC of the samples against photons generated with tube voltages of 40, 50, 60, 70 and 80 kVp. The LAC and MAC values decrease with increasing photon energy. The maximum and minimum LAC and MAC are observed at 40 and 80 kVp respectively, which is in consonance to the results reported in literature [22][23][24].

LACs were evaluated in a wide energy range to examine the behavior at higher energy levels. For all studied energies, the LAC values for any systems (doped with varying concentrations of leather) followed the following declining trend of LAC characteristics. And thus, with lower contraction of sand showed higher LAC values, Also the sample with zero (0) concentration of sand gives higher shielding ability. At the energy of 80 kVp, the LACs decreased. Sample S1 with the highest concentration of sand (50:50) for both sand and leather shows lower LAC and MAC values compared with the other samples, which is not correlation with higher concentration of dopants. Thereby suggesting that higher plastic concentration increases the shielding efficiency. The MAC and LAC value demonstrated by the sand reinforced plastic concrete presented in this work showed great shielding efficiency when compared with those of some concrete materials as presented in the work of Thakur et al.[25].

For a given thickness and density of material, the probability of interaction depends on the number of atoms the X-rays encounter per unit distance. The cross section of photoelectric absorption increases increased when the photo energy exceeds the binding energy of inner shell electrons. Thus, increasing the plastic concentration results in an increase in the number of electrons available for interaction. This process is very significant for high Z targets in diagnostic X-ray. From Figures 6, there is absorption edges in some samples (S₁ and S₂), which results in abrupt increase in the

attenuation coefficients in the blocks system 0:100 and 10:90 sand to plastic ratio as a result of k-edge energy at 70 – 80 kVp [26].

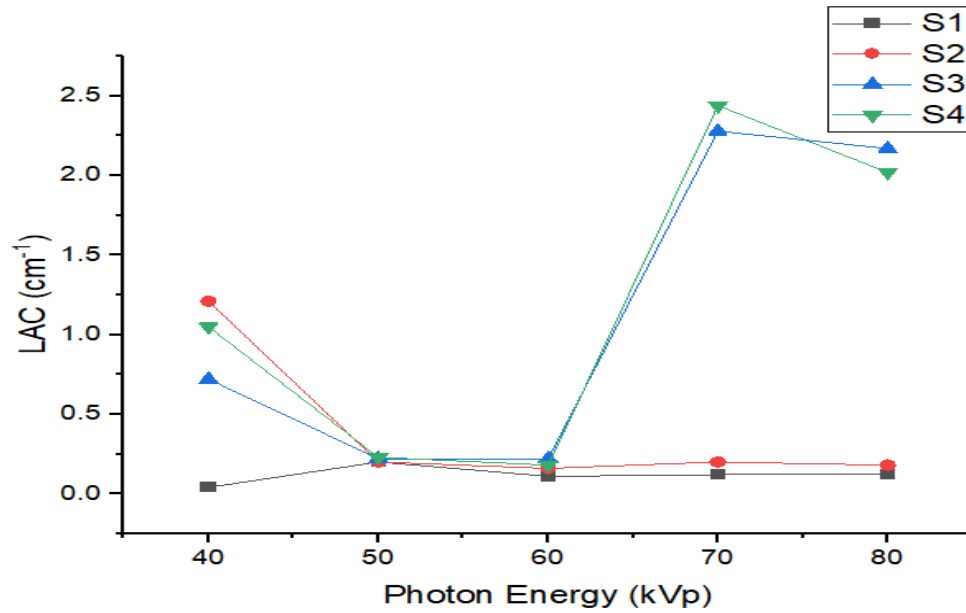


Figure 6: Linear Attenuation Coefficients as a Function of X-rays Photon Energy

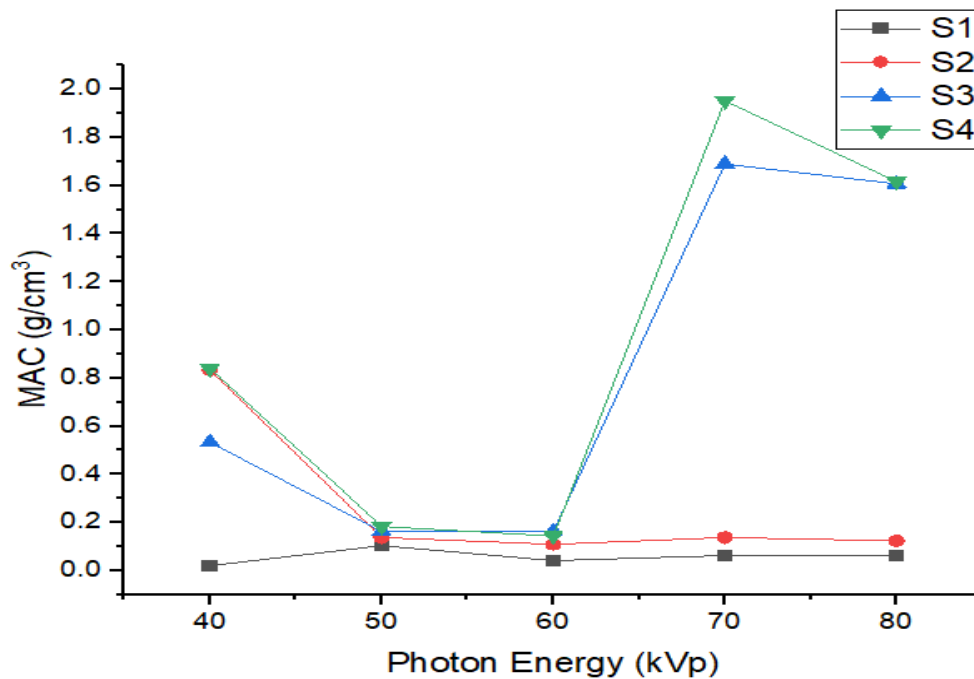


Figure 7: Mass Attenuation Coefficient as a Function of X-rays Photon Energy

Half and Tenth Value Layer

The thickness at which the transmitted intensity is reduced to 50% and 90% of the initial intensity is known as the Half Value Layer (HVL) and Tenth Value Layer (TVL), respectively. HVL and TVL are parameters of interest in shielding experiments. These parameters are computed using Equations (5) and (6) respectively [27] [27] [28].

Greater space conservation and improved radiation shielding efficacy are associated with lower HVL [28], [30]. The HVL and TVL of the new block are presented in Figures 4.4 and 4.5. In other words, HVL and TVL reveal their lowest values for lower sand concentration in the bricks.

High-energy photons have lower interaction cross sections with material atoms less frequently than the travel through the material matrix, and this results in an increase in HVL and TVL values. Accordingly, photons of lower photon energies, as seen in the data \ the block would have higher shielding efficiency [31], [32].

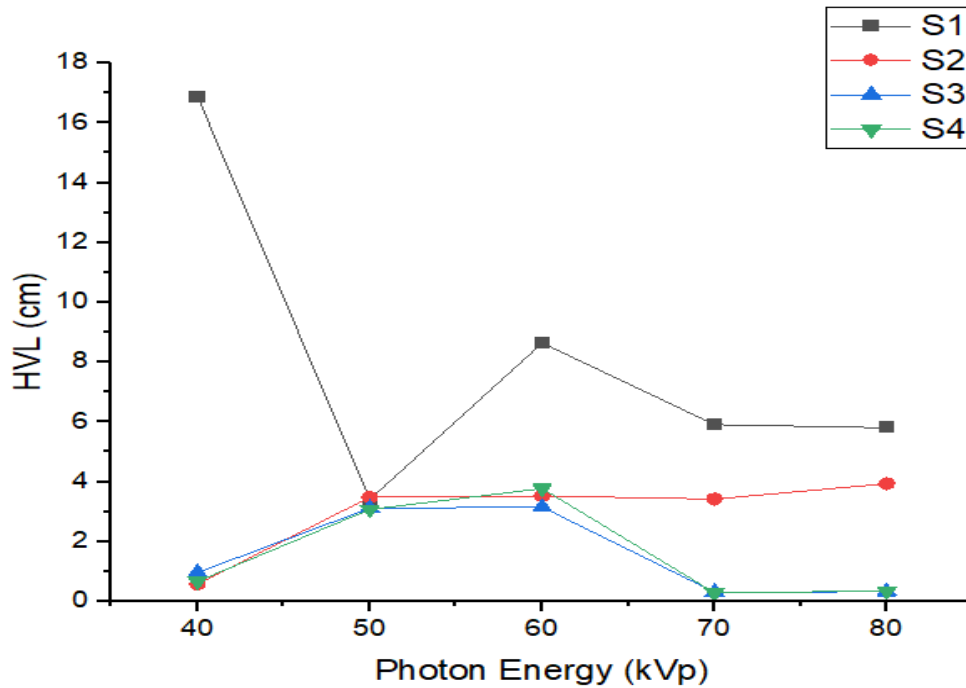


Figure 8: Half Value Layer as a Function of X-rays Photon Energy

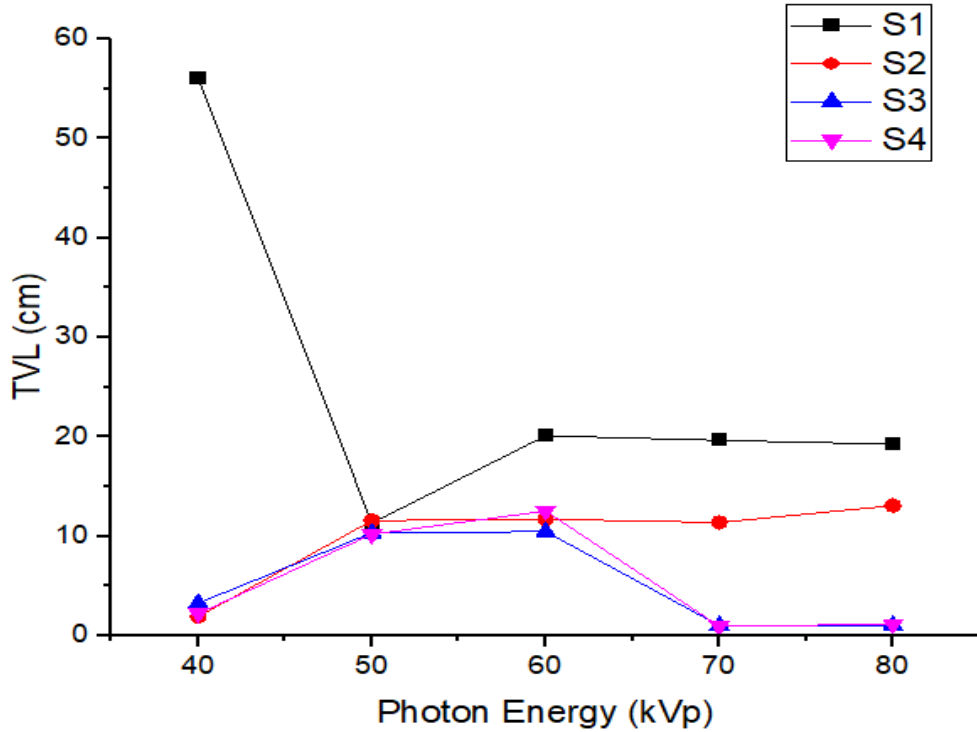


Figure 9: Tenth Value Layer (TVL) as a Function of X-rays Photon Energy

Mean Free Path

The mean free path (MFP), described as the mean distance through which the energetic photon moves after interaction [33]. It is the inverse of LAC, and it is measured in cm.

The mean-free path (MFP) of the blocks under study in the given photon energy range of 40 to 80 kVp is depicted in Figure 10. The MFP values range from 0.45 to 0.95 cm for 0:100 (S4) block and from 8.36 to 24.35 cm for 50:50 (S1) block. The least MFP are at lower energies and grow progressively with the increase in photon energy, as seen in Fig. 4.7. This is because high-energy radiation traverses easily through target materials.

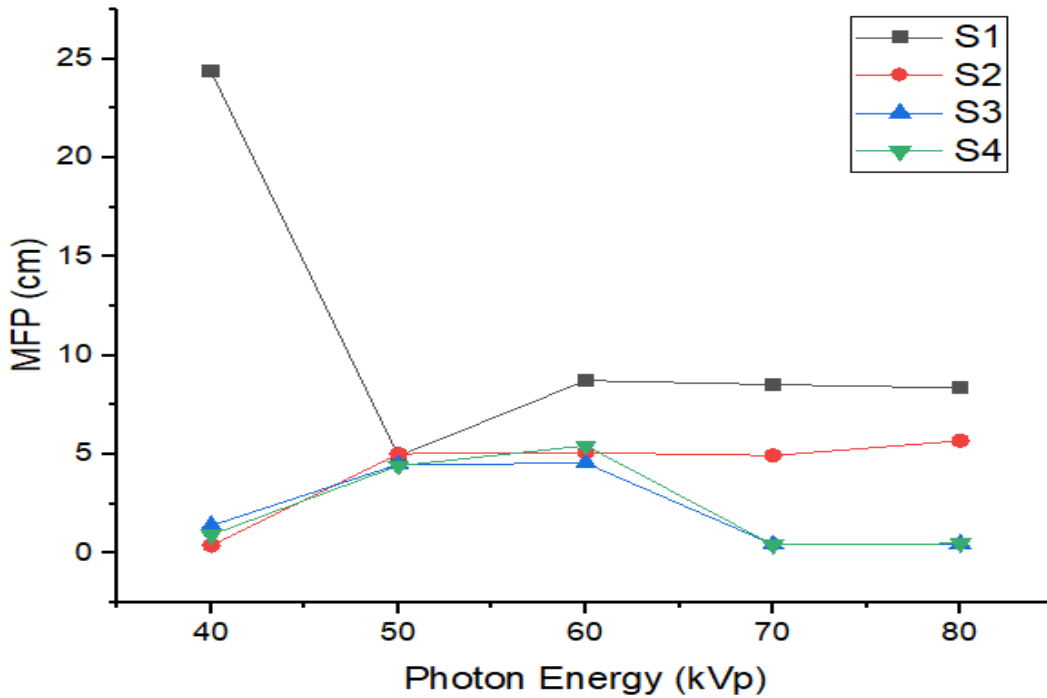


Figure 10: Mean-Free Path (MFP) as a Function of X-rays Photon Energy

These results are somewhat not related to the density of each block composition system because photons interact more with atoms of the denser material, causing an increased attenuation [31], [33]–[35]. In other words, increasing the dopant concentration (leather), results increase the interaction cross section as reported by [23][24]. This indicates that the lower the sand concentration the better the shielding.

Conclusions

This paper presents a study, on the X-rays shielding characteristics of sand reinforced plastic concretes fabricated using sand and waste sachet water plastic materials in percentage ratio of 50:50, 30:70, 10:90 and 0:100 sand and silica. Density measurement was performed using a digital densitometer device that works based on the Archimedes principle. The X-rays shielding characteristics of the synthesized sand reinforce plastic concrete blocks was measured using a combine system of fixed diagnostic x-ray machine (as X-rays source) and digital Geiger counter (as detector and dose counter). The density of the synthesized concrete blocks continued to decrease with increasing plastic percentage. The LAC and MAC values increased as the plastic composition increased from 50% to 100%. The HVL, TVL and the MFP values showed a decreasing pattern with an increase in the percentage of waste plastic material. The synthesized plastic based concrete blocks showed great efficiency in shielding X-rays and light weight. These quantities demonstrated that the studied material could solve the problem of durability and heaviness of the traditional cement based concrete material and thus will be good for X-ray rooms and nuclear centers construction.

References

- [1] H. A. Saudi, H. O. Tekin, H. M. H. Zakaly, S. A. M. Issa, G. Susoy, and M. Zhukovsky, "The impact of samarium (III) oxide on structural , optical and radiation shielding properties of thallium-borate glasses : Experimental and numerical investigation," *Opt. Mater. (Amst.)*, vol. 114, no. February, p. 110948, 2021, doi: 10.1016/j.optmat.2021.110948.
- [2] S. H. Alazoumi *et al.*, "Structural, elastic, thermo-physical and gamma radiation shielding efficiency of MnO₂ doped TeO₂-PbO-ZnO glasses," *Opt. Mater. (Amst.)*, vol. 150, no. January, p. 115277, 2024, doi: 10.1016/j.optmat.2024.115277.
- [3] M. G. Dong *et al.*, "Investigation of gamma radiation shielding properties of lithium zinc bismuth borate glasses using XCOM program and MCNP5 code," *J. Non. Cryst. Solids*, vol. 468, no. April, pp. 12–16, 2017, doi: 10.1016/j.jnoncrsol.2017.04.018.
- [4] A. Azuraida *et al.*, "GAMMA RAY SHIELDING PARAMETER OF BARIUM-BORO-TELLURITE GLASS," *Chalcogenide Lett.*, vol. 17, no. 4, pp. 187–196, 2020.
- [5] M. I. Sayyed, H. O. Tekin, E. E. Altunsoy, S. S. Obaid, and M. Almatari, "Radiation shielding study of tellurite tungsten glasses with different antimony oxide as transparent shielding materials using MCNPX code," *J. Non. Cryst. Solids*, vol. 498, no. April, pp. 167–172, 2018, doi: 10.1016/j.jnoncrsol.2018.06.022.
- [6] I. G. Geidam *et al.*, "Oxide ion polarizabilities and gamma radiation shielding features of TeO₂ – B₂O₃ – SiO₂ glasses containing Bi₂O₃ using Phy-X / PSD software," *Mater. Today Commun.*, vol. 31, no. April, pp. 1–9, 2022.
- [7] P. Kalla, A. Rana, Y. Bahadur, A. Misra, and L. Csetenyi, "Durability studies on concrete containing wollastonite," *J. Clean. Prod.*, vol. 87, pp. 726–734, 2015, doi: 10.1016/j.jclepro.2014.10.038.
- [8] M. G. Dong, R. El-Mallawany, M. I. Sayyed, and H. O. Tekin, "Shielding properties of 80TeO₂–5TiO₂–(15–x) WO₃–xAnOm glasses using WinXCom and MCNP5 code," *Radiat. Phys. Chem.*, vol. 141, no. May, pp. 172–178, 2017, doi: 10.1016/j.radphyschem.2017.07.006.
- [9] R. Kurtulus, T. Kavas, K. A. Mahmoud, and M. I. Sayyed, "A comprehensive examination of zinc-boro-vanadate glass reinforced with Ag₂O in physical, optical, mechanical, and radiation shielding aspects," *Appl. Phys. A Mater. Sci. Process.*, vol. 127, no. 2, pp. 1–13, 2021, doi: 10.1007/s00339-021-04282-6.
- [10] S. Mukamil *et al.*, "Lead-borate glass system doped with Sm³⁺ ions for the X-ray shielding applications," *Results Phys.*, vol. 43, no. November, p. 106121, 2022, doi: 10.1016/j.rinp.2022.106121.
- [11] A. B. Azeez, K. S. Mohammed, M. Mustafa, and A. Bakri, "Evaluation of Radiation Shielding Properties for Concrete with Different Aggregate Granule Sizes," no. May 2014, 2013.
- [12] A. M. Onaizi *et al.*, "Radiation-shielding concrete: A review of materials, performance, and the impact of radiation on concrete properties," *J. Build. Eng.*, vol. 97, no. September,

- p. 110800, 2024, doi: 10.1016/j.jobe.2024.110800.
- [13] A. B. Azeez *et al.*, “The Effect of Various Waste Materials’ Contents on the Attenuation Level of Anti-Radiation Shielding Concrete,” no. October, 2013, doi: 10.3390/ma6104836.
- [14] A. B. Azeez, K. S. Mohammed, A. M. M. Al Bakri, H. I. Hasan, and O. A. Abdulkareem, “Radiation shielding characteristics of concretes incorporates different particle sizes of various waste materials,” no. April 2014, 2013, doi: 10.4028/www.scientific.net/AMR.925.190.
- [15] A. B. Azeez *et al.*, “The Effect of Various Waste Materials’ Contents on the Attenuation Level of Anti-Radiation Shielding Concrete,” no. July, 2013, doi: 10.3390/ma6104836.
- [16] H. E. J. Koskinen and E. K. J. Kilpua, “Radiation Belts and Their Environment,” in *Physics of Earth’s Radiation Belts*, 2022, pp. 1–25.
- [17] A. S. Aliyu *et al.*, “Optoelectronic and Gamma Ray Attenuation Properties of Ore-based Bi and Sn-doped Borosilicate Glasses,” *Ceram. Int.*, vol. 50, no. 15, pp. 26424–26434, 2024, doi: 10.1016/j.ceramint.2024.04.369.
- [18] J. Kaewkhao, M. Djamal, and T. Korkut, “Interaction of radiation with matter and related topics,” *Science and Technology of Nuclear Installations*, vol. 2014. Hindawi Publishing Corporation, 2014. doi: 10.1155/2014/207484.
- [19] A. Alessio *et al.*, “Produced with the kind Support of Radiation Protection and Dose Optimisation A Technologist’s Guide.”
- [20] R. El-Mallawany and M. I. Sayyed, “Comparative shielding properties of some tellurite glasses: Part 1,” *Phys. B Condens. Matter*, vol. 539, no. April 2017, pp. 133–140, 2018, doi: 10.1016/j.physb.2017.05.021.
- [21] S. Kaewjaeng, S. Kothan, N. Chanthima, H. J. Kim, and J. Kaewkhao, “Gamma radiation shielding materials of lanthanum calcium silicoborate glasses,” in *Materials Today: Proceedings*, Elsevier Ltd, 2018, pp. 14901–14906. doi: 10.1016/j.matpr.2018.04.027.
- [22] S. Kaewjaeng, K. Boonyu, H. J. Kim, J. Kaewkhao, and S. Kothan, “Study on radiation shielding properties of glass samples doped with holmium,” *AIP Conf. Proc.*, vol. 2279, no. 1, p. 60005, 2020.
- [23] S. Sarachai, N. Chanthima, N. W. Sangwanatee, and S. Kothan, “Radiation Shielding Properties of BaO-ZnO-B₂O₃ Glass for X-Ray Room,” vol. 766, pp. 88–93, 2018, doi: 10.4028/www.scientific.net/KEM.766.88.
- [24] A. S. Aliyu *et al.*, “Bismuthite and cassiterite-doped borosilicate glass systems for X-rays attenuation : Fabrication and characterisation,” *Opt. Mater. (Amst)*, vol. 151, no. April, p. 115365, 2024, doi: 10.1016/j.optmat.2024.115365.
- [25] S. Thakur *et al.*, “Thermo- and photoluminescent properties and gamma radiation shielding efficiency of NiO doped B₂O₃–Bi₂O₃ glass system,” *Radiat. Phys. Chem.*, no. xxxx, 2023.

- [26] Y. A. Abdelghany, M. M. Kassab, M. M. Radwan, and A. Abdel-Latif M, "Investigation of optical, mechanical, and shielding properties of zirconia glass capsule," *Prog. Nucl. Energy*, vol. 154, Dec. 2022, doi: 10.1016/j.pnucene.2022.104457.
- [27] U. Periřanođlu, F. I. El-Agawany, E. Kavaz, M. Al-Buriahi, and Y. S. Rammah, "Surveying of Na₂O₃–BaO–PbO–Nb₂O₅–SiO₂–Al₂O₃ glass-ceramics system in terms of alpha, proton, neutron and gamma protection features by utilizing GEANT4 simulation codes," *Ceram. Int.*, vol. 46, no. 3, 2020, doi: 10.1016/j.ceramint.2019.10.023.
- [28] E. M. A. H. A. M. Madbouly, "Chemical and radiation shielding effectiveness of some heavy metal oxide glasses for immobilizing radioactive wastes," *J. Aust. Ceram. Soc.*, no. 0123456789, 2023, doi: 10.1007/s41779-023-00951-2.
- [29] Z. . Dong, M., Xue, X., Yang, H., Liu, D., Wang, C., Li, "A novel comprehensive utilization of vanadium slag: as gamma ray shielding material.," *J. Hazard. Mater.*, vol. 318, pp. 751–757, 2016.
- [30] M. I. Sayyed, M. G. Dong, H. O. Tekin, G. Lakshminarayana, and M. A. Mahdi, "Comparative investigations of gamma and neutron radiation shielding parameters for different borate and tellurite glass systems using WinXCom program and MCNPX code," *Mater. Chem. Phys.*, vol. 215, 2018, doi: 10.1016/j.matchemphys.2018.04.106.
- [31] B. V. Kheswa, "X-ray shielding properties of bismuth-borate glass doped with rare earth ions," 2023.
- [32] M. A. M. Uosif *et al.*, "Lead-Free Ternary Glass for Radiation Protection : Composition and Performance Evaluation for Solar Cell Coverage," 2023.
- [33] M. S. Alqahtani *et al.*, "Structural and performance radiation protection the phosphate glasses contain: Te, K, Al, Nb-doped with rare earth," *Chalcogenide Lett.*, vol. 20, no. 1, pp. 43–54, 2023, doi: 10.15251/CL.2023.201.43.
- [34] D. A. Aloraini *et al.*, "Preparation, radiation shielding and mechanical characterization of PbO–TeO₂–MgO–Na₂O–B₂O₃ glasses," *Radiat. Phys. Chem.*, vol. 198, p. 110254, Sep. 2022, doi: 10.1016/J.RADPHYSICHEM.2022.110254.
- [35] A. H. Almuqrin, M. Elsafi, S. Yasmin, and M. I. Sayyed, "Morphological and Gamma-Ray Attenuation Properties of High-Density Polyethylene Containing Bismuth Oxide," *Materials (Basel)*, vol. 15, no. 18, pp. 1–11, 2022, doi: 10.3390/ma15186410.